07.01.2016

The 2009–2010 step in atmospheric CO_2 inter-hemispheric difference

R. J. Francey and J. S. Frederiksen

{CSIRO Oceans & Atmosphere, Aspendale, Victoria, Australia}

Correspondence to: R. J. Francey (roger.francey@csiro.au)

Abstract

The annual average CO_2 difference between baseline data from Mauna Loa and the Southern Hemisphere increased by ~0.8 μmol mol^{-1} (0.8 ppm) between 2009 and 2010, a step unprecedented in over 50 years of reliable data. We find no evidence for coinciding, sufficiently large source/sink changes. A statistical anomaly is unlikely due to the highly systematic nature of the variation in observations. An explanation for the step, and the subsequent 5 year stability in this north–south difference, involves inter-hemispheric atmospheric exchange variation. The selected data describing this episode provide a critical test for studies that employ atmospheric transport models to interpret global carbon budgets and inform management of anthropogenic emissions.

1 Introduction

The record 2009–2010 increase in annual mean CO_2 difference between hemispheres, $\Delta C_{N\text{-}S}$, was reported by Francey et al. (2013) using data from Mauna Loa (mlo, 20°N, 156°W, altitude 3.4 km) and Cape Grim (cgo, 41°S, 145°E, 0.2 km) or South Pole (spo, 90°S, 2.8 km). In the context of seeking an explanation for decadal differences between the fossil emission trends and trends in atmospheric CO_2 growth rate, they attempted an empirical correction for reported natural influences on CO_2 growth using multiple regression of reported wild fires, volcanoes and El Nino–Southern Oscillation (ENSO) with CO_2 records. None of these reported influences showed statistically significant anomalous behaviour in the 2009–2010 period.

A Commonwealth Scientific and Industrial Research Organisation (CSIRO) inversion which deduces surface fluxes from atmospheric CO_2 observations is based on atmospheric transport descibed by the Cubic Conformal Atmospheric Model (CCAM, McGregor and Dix, 2008). This explains the 2009–2010 ΔC with a 2010 Northern Hemisphere (NH) source in the Asian region, distributed widely enough to be unverifiable by “bottom-up” methods (Rachel Law, private communication).

However, Poulter et al. (2014), using a terrestrial biogeochemical model, atmospheric carbon dioxide inversion and global carbon budget accounting methods, suggested that the $\Delta C_{mlo\text{-}cgo}$ step might be explained by a record 2011 land carbon sink located in the semi-arid regions of the Southern Hemisphere (60% of which was in Australia).

Furthermore, Patra (2015) demonstrated consistency in 2009-2010 between their ACTM simulations of $\Delta C_{mlo\text{-}cgo}$ and fluxes obtained from an inversion model. However, from the limited information available, it seems likely that both the $\Delta C_{mlo\text{-}cgo}$ and the inversion fluxes are dependent on the same transport parameterisations, and so are not independent. His comment prompts a question about the effectiveness of SF_6 measurements to "diagnose" model CO_2 inter-hemispheric transport.

In order to address the apparent conflicts, we update CO_2 measurements and search more widely for concurrence with independently determined parameters, including other trace gas species and atmosphere physical parameters influencing their distribution.

We are informed by a companion paper examing potential bias in the two largest terms in a global carbon budget (Francey et al., 2016). They document significant reductions in susceptibility to bias in atmospheric CO_2 measurements since the 1990s and express concern about spatial representation of reported CO_2 measurements, e.g. in monthly averaged data. Mismatch between the inversion model gridscale and the scale of CO_2 representativeness at observing sites can introduce significant uncertainty in inversion modelling that may act to obscure large-scale systematic CO_2 behaviour.

2 Updated CO_2 Data

Inversions of CO_2 data effectively interpret CO_2 spatial and temporal differences in terms of surface exchanges. Thus, Figure 1 illustrates each type of difference, namely $\Delta C_{N\text{-}S}$ and dC/dt, in quality data with maximum spatial representation. Methods to obtain $\Delta C_{N\text{-}S}$ and dC/dt from monthly flask data are descibed in Appendix A.

The updated spatial comparisons of $\Delta C_{N\text{-}S}$ in Fig. 1a highlight the largely consistent results from the 1990s using data from flask samples collected and measured by the CSIRO, by the National Oceanic and Atmospheric Administration (NOAA, Dlugokencky et al., 2014) and by the Scripps Institution of Oceanography (SIO, Keeling et al., 2009) networks. For perspective, a comparison is also made with a linear regression through the SIO 5-decade $\Delta C_{mlo\text{-}spo}$ record. This shows an overall increase, generally attributed to the increase in Fossil Fuel (FF) emissions (Boden et al., 2010), which occur predominantly in the NH.

Annual global FF, including the Francey et al. (2013) suggested correction, are scaled and included to run parallel to the ΔC slope in Fig. 1a in order to emphasize the unusual magnitude of the 2009–2010 ΔC step. From this perspective the 0.8 ppm step, if the result of an anomalous flux, would equate to an annual 1.6 PgC (NH) source, one sufficiently large and rapid that detection by bottom-up studies might be expected.

Also in Fig. 1a, the unusual post-2009 ΔC stability compared to the earlier record is obvious. Since methodologies have not significantly changed over this period it suggests that measurement error is not a factor and the variability in the pre-2010 $\Delta C_{N\text{-}S}$ data is not random.

The temporal differences, d*C*/d*t* in Fig. 1b, show inter-annual variability on 3 to 5 year El Niño–Southern Oscillation (ENSO) timeframes. Using CCAM transport to invert CO_2 and $\delta^{13}CO_2$ observations, Rayner et al. (2008) concluded that it is forced primarily by climate variability on the equatorial land biosphere. This conclusion is consistent with the observation of limited influence on ΔC for equatorial exchanges in Fig. 1b, to be discussed further below. However the question of spatial representativeness of the selected CO_2 records is addressed first.

The hemispheric representativeness of baseline data from the mlo and cgo monitoring sites is supported by a study of aircraft vertical profiles at 12 global sites conducted in maximum convective conditions near midday (Stephens et al., 2007). The lower levels (<1-2 km) of all 12 vertical profiles exhibited seasonal variation resulting from climate influence on regional surface carbon reservoirs. The amplitudes of the seasonal variation at mlo and cgo are the least in their respective hemispheres, which aids definition of inter-annual variability at these sites.

While the spo data closely track cgo data, and other mid-to-high southern latitude (SH) sites in the CSIRO network (Francey et al., 2013), the situation is less clear for mlo because of NH heteorogeneity and downwind proximity to Asia. A possible recent contributing factor at mlo may result from geographical susceptibility to rapidly increasing SE Asian pollution, “rapidly transported to the deep tropics” (Ashford et al., 2015). In Figure 2 we demonstrate similarity in year-to-year changes in ΔC using both Pacific and Atlantic extra-tropical NH sites from the NOAA network. The similarity is particularly significant in sign and magnitude for the two largest observed changes in 2009–2010 and 2002–2003, implying that especially for these periods mlo represents NH behaviour.

During 2009–2010, dC/dt show a larger NH ENSO peak, leading that in the SH by around 6 months, a phase difference not observed for other significant El Niño peaks in Fig. 1b. This implies either an undetected NH source, or possibly, rapid changes in inter-hemispheric (IH) transport.

Poulter (2015) raises the issue of relative timing of the ΔC step and the response of SH savanna regions to the end of drought. To clarify this we include Figure 3, showing CSIRO monthly baseline concentrations at mlo and cgo through the period. To aid discussion, the seasonal variations are compared to quadratic fits to the 1992–2014 data for each site, offset by ± the long term amplitude of the seasonality, ± 3.3 ppm (6.6 ± 0.5 ppm peak-to-peak) at mlo and ± 0.55 ppm (1.10 ± 0.2 ppm p-p) at cgo.

There is a change in the mlo seasonality (the 2009 seasonal amplitude is the smallest and the 2010 amplitude the largest in this plot) between 2009 and 2010 which is of a sign and magnitude that most easily explains the 0.8 ppm step in annual average differences, $\Delta C_{mlo\text{-}cgo}$. Slightly lower CO_2 in the cgo baseline data in the 2010–2012 period could possibly be associated with a SH sink. However, the unusually large negative seasonal excursion from the mean, at the end of the 2009–2010 spring-summer uptake season, is before the October 2010 to March 2011 record floods in Northern Australia which were identified as a trigger for the savanna response by Poulter et al. (2014); furthermore the negative dip is followed by a near-average positive seasonal excursion in late 2010. Conventional descriptions of the Cape Grim seasonality have contributions from SH biosphere, seasonal SH ocean temperature changes and ~6-month delayed NH biosphere signals (Law et al., 2006; Stephens et al., 2013); failure of a delayed NH signal to reach Cape Grim might also contribute to low SH autumn CO_2 at Cape Grim. Nevertheless, a small contribution from a SH terrestrial sink is difficult to exclude in 2011 and 2012.

This question was further addressed at the 2014 Annual Cape Grim Science Meeting by Xingjie Lu, Ying-Ping Wang and Rachel Law (Ying-Ping Wang, Rachel Law, personal communications). They used the Community Atmosphere Biosphere Land Exchange model (CABLE, Law 2014) to simulate Net Ecosystem Production anomalies over the 2001 to 2012 period, finding SH anomalies that were mainly contributed by Argentina and Australia in 2010 and 2011. The timing of their terrestrial response is similar to that of Poulter et al. (2014). They investigated how the inter-annual variability in the CABLE biospheric fluxes affected $\Delta C_{mlo\text{-}cgo}$

using CO_2 response functions from the CCAM atmospheric model. When the CCAM CO_2 response functions are modified to represent baseline data (at cgo the 20-30% of time with strong winds over the southern ocean) this terrestrial signal is sufficiently diluted into the large well-mixed troposphere at mid-to-high southern latitudes to be reduced to insignificance in the reconstructed $\Delta C_{mlo-cgo}$. With their approval, the relevant CCAM modelling runs are included in Supplementary Information. This example highlights a requirement for high time resolution transport modelling coupled with similar resolution in the CO_2 data if such events are to be correctly attributed.

Finally, independent evidence for the NH origin of the 2009 to 2010 CO_2 ΔC step comes from a recent analysis of upper troposphere measurements for 11 latitude bands between 30°N to 30°S (Matsueda et al., 2015) where the step is evident north of 10°N. These authors suggest a role for transport, as well as source/sinks, to explain their year-to-year variations in latitudinal differences.

3 Responses in ΔC and dC/dt to Other Recent Source/Sink Anomalies

Before examining a likely role of atmospheric transport in ΔC variations, we briefly examine Fig. 1 at the times of the major post-1992 independently-documented anomalous CO_2 source/ sink activity: the 1997–1998 Indonesian peat fires, the 2002–2003 NH drought and boreal wildfires, and the 2008 Global Financial Crisis.

- The 1997–1998 Indonesian peat fires correspond to the largest El Nino peak dC/dt, and was estimated as contributing around 1 Pg C (6.5 times the mean Equatorial Asia emissions) to the atmosphere in 1997 (Page et al., 2009; Giglio et al., 2013). In Fig. 1 there is a small increase in ΔC_{N-S}, with a barely significant larger NH dC/dt peak. A small response might be explained if the emissions are mixed into both hemispheres. The possibility that changes in IH mixing may also contribute to ΔC_{N-S}, is discussed below.
- While the 2002–2003 ΔC_{N-S} in Fig. 1a is the second largest year-to year-increase (see also Fig. 2), it is also the largest difference in dC/dt between the hemispheres. Year 2003 corresponds to drought in Europe "un-precedented during the last century", releasing ~0.5 PgC yr^{-1} (Ciais et al., 2005), adding to 2003 GFED4 fire emissions in boreal

America and boreal Asia of 0.31 PgC, 2.5 times the 1997-2013 mean (Giglio et al., 2013). However for emissions spread evenly over a full year, a relatively small ΔC impact is expected since the 2003 NH FF combustion was ~7.5 PgC compared to < 0.7 PgC from the non-FF sources.

- The Global Financial Crisis (GFC) of 2007–2008 (Peters et al., 2012) coincides in Fig. 1b with the only occasion when the NH dC/dt ENSO peak is markedly smaller than that in the SH. While 2008, 2009 are the two lowest global fire emission years in the GFED4 database, combined boreal emissions are near average, favouring the GFC as a more likely explanation for the dC/dt behaviour. However, it is less clear that relatively low 2008, 2009 ΔC in Fig. 1a are attributable to the GFC, and a possible contribution from IH exchange is also examined below.

4 Anomalies in Annual Interhemispheric Mixing

Meridional transport and eddy mixing due to large scale eddy motions are sources of significant uncertainty in estimations of IH transport (Miyazaki et al., 2008). Here we examine the role of the opening and closing of the upper tropospheric equatorial westerly duct, and associated inter-hemispheric Rossby wave propagation, as a contributor to the 2009–2010 $\Delta C_{mlo\text{-}cgo}$ shift, and other variations, shown in Fig. 1a.

Extra-tropical NH Rossby waves, including a branch of the Himalayan wave-train, are able to penetrate into the SH when near-equatorial zonal winds are westerly in the upper tropospheric duct centred on 140W to 170W and 5N to 5S (Webster and Holton, 1982; Frederiksen and Webster, 1988; Webster and Chang, 1988). This region is delineated and its tropospheric relevance revealed in Fig. 4a showing strongly correlated upper tropospheric westerly winds with the Southern Oscillation Index (SOI) over the full 1949 to 2011 wind reanalysis dataset (http://www.esrl.noaa.gov/psd/data/gridded/data.ncep.reanalysis.html).

The wind direction and strength (u_{duct}) in this duct are determined by seasonal and ENSO sea-surface temperature variations; the upper troposphere westerlies are strongest in the boreal winter, and during La Nina periods, when they are correlated with proportional increases in near-equatorial transient kinetic energy (Fig. 6, Frederiksen and Webster, 1988) which facilitates inter-hemispheric mixing of trace gases. At other times, including El Ninos, the u_{duct}

are near zero or easterly, causing the Rossby wave eddies to be deflected northwards and dissipated in the equatorial regions, inhibiting inter-hemispheric exchange.

For the period July 2009 to June 2010 the average 300hPa equatorial zonal winds in the duct region were easterly as shown in Fig. 4c, effectively closing the duct and increasing the build-up of FF CO_2 in the NH. The July 2008 to June 2009 open duct pattern, with westerlies in the duct, is shown in Fig. 4d. (Appendix C addresses the altitude range involved in this process. Note also, the meridional wind may make a small contribution to IH transport in the duct region during this time).

Fig. 4b shows the 300hPa zonal winds for July 2008 to June 2009 (Fig. 4d) minus those for July 2009 to June 2010 (Fig. 4c) and the pattern bears strong similarities with the long-term zonal wind versus SOI correlation in Fig. 4a.

5 Trace gas interhemispheric exchange through the duct

Inter-hemispheric exchange of a seasonally varying gas by this process depends on co-variance with u_{duct}, and is represented in Figure 5 by the product of monthly u_{duct} and ΔC for routinely monitored CSIRO species C= CO_2, CH_4, CO and H_2. The direction of a step in ΔC depends on the magnitude and sense of the trace gas IH gradient when the duct is open. The seasonality at mlo and cgo for the different gases are given in Supplementary Information.

In the top panel monthly u_{duct} are plotted over red and blue shading representing El Niño and La Niña periods respectively. We add symbols connected by a solid line that are an integration of the NH winter peaks, Σu_{duct} (October to April) for a nominal $u_{duct} > 2$ ms^{-1}, in order to better compare year-to-year changes in the strength and duration of the seasonal duct exchange.

Fig. 1 is re-examined in the light of variations in Σu_{duct}. Of the seven lowest Σu_{duct} in Fig. 5, 1992, 1995, 1998, 2003, 2005, 2007 and 2010, six correspond to peak $\Delta C_{mlo-cgo}$ in CSIRO data. Differences between laboratories are more marked before the mid-1990s in Fig. 1a, marking a period of significant improvement in inter-laboratory quality monitoring (e.g. Masarie et al., 2001) but also influenced by the major perturbation to the carbon cycle associated with the 1991 Pinatubo eruption. However the relationship with Σu_{duct} is, in the main, supported by SIO and NOAA data.

The two extreme cases of duct closure (Σu_{duct} <10 ms^{-1}) since 1992 in Fig. 5 are in 1997/98 and 2009/10, showing up as a marked absence of a seasonal IH exchange ($\Delta C.u_{duct}$) for CO_2, CH_4 and CO. If the Fig. 1a ΔC step in 2009/10 is attributed to duct closure then a similar ΔC change might be expected in 1997/98, however it is less than half that in 2009/2010. The record CO_2 response to the 1997/98 equatorial anomaly, associated with prolonged equatorial peat combustion (Section 3), is a possible explanation for a smaller response. The next lowest seasonally integrated Σu_{duct} ~ 10 ms^{-1} in 2003, has the next largest ΔC increase in Fig. 1a and Fig. 2, strongly suggesting reduced seasonal IH transport. This complicates surface flux estimates from the inversion of CO_2 spatial differences by Rayner et al. (2008).

Switching focus to the positive excursions in Σu_{duct}, these are associated with increased strength of mixing through the open duct. Compared to previous behaviour, the magnitude of exchange ($\Delta C.u_{duct}$) immediately after the exended duct closure from July 2009 to June 2010 is the largest for each gas in Fig. 5, in part reflecting the fact that 2010–2011 La Niña corresponds to the most intense Σu_{duct} since 1990 (top panel Fig. 5). The unusual species exchange at this time is most marked for CO_2 and H_2, which we mainly attribute to the fact that these two gases exhibit the most significant ΔC trend (CO_2 positive, H_2 negative) over the two decades; also each has seasonal concentration amplitudes that are the largest compared to mean annual IH gradients (Supplementary Information).

Through the four "duct-open" periods after 2010, Fig. 1a shows ΔCO_2 to be practically constant, a phenomena difficult to explain with known source/sink behaviour. During this period Σu_{duct} monitonically decreases; the constant ΔC might be explained if the decreasing Σu_{duct} are matched by decreases in the annual fossil fuel emission increments. Boden et al. (2012) estimate the annual increments in FF to be 0.5 PgC in 2010, 0.3 PgC in 2011 and 0.2 PgC in 2012, supporting this interpretation.

6 Isotopic evidence of systematic ΔC variations

While covariance between atmospheric transport and terrestrial biosphere activity referred to as the "rectifier effect" is an important component in global carbon budgeting (Denning et al., 1999), it concerns seasonal variations in the depth of the atmospheric boundary layer rather than the abrupt upper atmosphere transport through the duct described by Fig. 5.

Measurements of the stable carbon isotope in atmospheric CO_2 have the potential to clarify the relative importance of modes of atmospheric behaviour on ΔC. This depends on the fact that an atmospheric $^{13}CO_2$ anomaly is redistributed in the environment more rapidly than a $^{12}CO_2$ anomaly, Tans et al. (1993). This isotopic equilibration process is facilitated by the large gross turnover of CO_2 with oceanic and terrestrial reservoirs. It can reflect the elapsed time since an emission anomaly occurred, and is examined below by comparing monthly with annually averaged data.

Measurements of the ratio of stable carbon isotopes, $^{13}C/^{12}C$, in atmospheric CO_2 are described by a reduced ratio $\delta^{13}C$ expressed in ‰; the ^{13}C content can be conveniently represented by the product C. $\delta^{13}C$, see Appendix B.

The dominant hemispheric CO_2 emissions are NH FF combustion and forest respiration. They each contain carbon that has undergone similar discrimination against the heavier isotope during photosynthesis. These sources are more-depleted in ^{13}C content than other possible sources, e.g. using Lloyd & Farquhar (1994) estimates of global discrimination relative to ambient atmospheric CO_2, forest carbon is globally ~ 18 ‰ lighter, savanna grasses are 4 ‰ lighter, and ocean carbon is in close equilibrium. (e.g. -18 ‰ equals -1.8 %).

Despite having similar isotopic composition, the imprint of recent forest exchange and FF emissions on atmospheric $\delta^{13}C$ can be different. A convenient demonstration uses the direct monthly relationship between $\delta^{13}C$ and C (only valid over small ranges of C), which in the NH is characterized by -0.05 ‰ ppm^{-1} and, since the seasonal variation in the SH is small, this relationship exists for monthly NH-SH $\Delta\delta^{13}C$. On annual timescales the C and $\delta^{13}C$ seasonal variations are largely cancelled, with negligible contribution to IH differences and ΔC changes are dominated by the steadily accumulating NH FF emissions that have greater opportunity for isotopic equilibration, which is evidenced over the last two decades by the observed mlo-cgo annual average $\Delta\delta^{13}C / \Delta C$ of -0.027 ± 0.003 ‰ ppm^{-1}.

Significant in the present context however, over the limited excursion range of annually averaged CSIRO pre-2010 data NH-SH $\Delta\delta^{13}C = -0.050(\pm 0.004)\Delta C + 0.062$ ‰ ($r^2 = 0.92$), identical to the monthly co-variations in $\Delta\delta^{13}C$ and suggesting involvement of un-equilibrated forest CO_2.

Francey et al. (2013) reported a synchronous decrease in stable carbon isotope ratio at the time of the 2009–2010 ΔCO_2 increase, measured in the same flask air samples. Those data are updated in Figure 6 and provided as Supplementary Information.

Fig. 6 plots the relative IH spatial changes in ^{13}C, represented by ($C.\delta^{13}C_{NH} - C.\delta^{13}C_{SH}$), compared to those in ^{12}C (using C_{NH-SH}, since C is 99% ^{12}C) in the CSIRO, NOAA and SIO samples used in Fig. 1a. All three data sets, and particularly CSIRO, show a linear relationship including the pre-2010 scatter, the 2009–2010 step, and subsequent data. The slope of the linear regressions represents the sum of source discrimination and ambient atmospheric $\delta^{13}C$ (Enting et al., 1993; Enting 2006).

Thus with the Lloyd and Farquhar estimate of global forest discrimination of -18 ‰ and an atmospheric value of -8 ‰ (e.g. the seasonal minimum at mlo in 2009/10), the -26.1 ‰ slope for the CSIRO data is near the most negative anticipated value, excluding significant influences of other possible CO_2 sources such as savanna grasses, and excluding significant isotopic equilibration that occur on longer than seasonal timeframes, all of which result in less negative slopes. These data strongly favour a major role for the duct transfer mechanism, for both the step and prior variability, since it occurs close to the seasonal CO_2 peak ($\delta^{13}C$ minimum) of NH terrestrial biosphere respiration in Fig. 5.

The relationship is far less well-defined in the NOAA and SIO data with regression slopes of -20 ‰ and -17 ‰, which, while both favouring C3 sources, do not exclude significant contributions from other sources, including annually-distributed, equilibrated FF CO_2. Note however, that if the 2009–2010 step was due to savanna grasses, then the post-2010 points (to the far right) in Fig. 6 would not fit on the two-decade regressions of any of the three data sets, since the anticipated slope for savanna exchange is around -12 ‰.

The NOAA and SIO data exhibit more scatter, with linear regression residual mean square scatter of 5, 11 and 17 ppm.‰ for CSIRO, NOAA and SIO plots, respectively. A lack of correlation in $\Delta\delta^{13}C$ variations between the NOAA and SIO, suggests that, whatever the IH transport mechanism, isotopic measurement precision is a more limiting factor in these datasets. By comparison, as befits a SH focus, precision has been a greater concern in CSIRO measurement programs, resulting in extensive published quality control assessments of the CSIRO isotope data since 1992, described in Appendix B, and supporting our preference for these data.

The intermittent nature of this IH exchange process might be expected to show up in other species like SF_6, used by the modelling community to diagnose IH transport (Patra, 2016). We address this issue in Appendix C. Incidentally, the estimate of possible co-variance between $\delta^{13}C$ and gross terrestrial primary productivity (Randerson et al., 2002) is likely to be impacted if a significant portion of IH exchange is via the upper atmosphere equatorial duct.

7 Historic evidence for anomalous interhemispheric CO_2 exchange

Fig. 7 examines the historic SIO mlo-spo records for responses to five other extended periods of duct-closure since the 1960s. Working backwards in time, there are seven occasions (circled in the top panel) when the seasonal $\Sigma u_{duct} < 5$ ms^{-1}. The five of these that correspond to an El Niño period closely followed by a La Niña (or in the case of 1982–1983 a weak La Niña shortly followed by a stronger one) show prominent peak values in ΔC (circled bottom panel); the two low Σu_{duct} not coinciding with a ΔC peak (smaller circles) have relatively brief El Niño periods not followed by La Niña. While there are two small ΔC peaks prior to 1970, the ΔC are more susceptible to missing data (particularly at spo*)* and measurement bias (Francey et al., 2016), and NCEP data may be less reliable, so are not considered further here. The 1986–88 event most mirrors 2009–10 being the next largest step, followed by four years of relatively stable ΔC.

We conclude from this that anomalies in the inter-hemispheric exchange through the duct have played a significant ongoing role in modifying spatial differences in CO_2 (and other trace species) at the surface. As NH FF CO_2 emissions increase further, the influence is expected to become more marked in $\Delta C.u_{duct}$.

8 Conclusions

Peylin et al. (2013) describe conflict between groups of carbon budgeting models in locating the major global terrestrial sink, whether mid-northern latitude or equatorial, and suggest atmospheric transport implementations may be involved. We have presented a variety of complementary evidence, including CO_2 isotopes, linking interhemispheric transport through the Pacific upper troposphere equatorial duct and the spatial and temporal difference in measured surface CO_2 concentrations. The observed patterns of CO_2 inter-hemispheric changes

are not easily explained by observed source/sink behaviour. If the parameterisations of transport in the global carbon budget models do not adequately capture the duct process, then spatial differences arising from transport are most likely to be interpreted as variation in terrestrial sinks. It also suggests that the SH seasonality in CO_2 may have been misinterpreted. For example when the duct is open, the January to April IH exchange through the duct will offset the spring minimum CO_2 level due to SH terrestrial uptake. The conventional explanation has a ~6 month delayed exchange arriving in the SH autumn and enhancing peak SH respiration. Global budgeting of other trace gas studies (e.g. Locatelli et al., 2013) are also likely to be impacted.

The observed 2009–2010 changes in CO_2 IH difference in particular, because of the magnitude and also the absence of plausible reported source/sink changes (in a time of unprecedented monitoring of ecosystem and ocean exchanges), provide an unusual opportunity to test the implementation of atmospheric transport in inversion models and help remove current ambiguities between surface exchanges and transport. More generally, this requires such models to demonstrate an ability to describe the spatial and temporal sytematic differences in selected high-quality baseline trace gas records that have well established large-scale representation, such as the mlo-cgo records used here.

Author Contribution: RJF proposed this study and provided trace gas information, and JSF the atmospheric dynamics information.

Acknowledgements

We are grateful to Anonymous Referee #1, Prabir Patra and Ben Poulter for their constructive criticism of the Discussion Paper. The paper relies on the decades-long commitment by skilled CSIRO GASLAB scientific personnel, particularly Paul Steele, Ray Langenfelds, Paul Krummel, Colin Allison, Paul Fraser and Marcel van der Schoot. Many support staff in GASLAB, Cape Grim Baseline Air Pollution Station (The Australian Bureau of Meteorology with CSIRO), and measurement collaborators at NOAA, also contribute directly in this regard.

07.01.2016

The importance of the historic SIO records cannot be understated. Rachel Law provided global, and Ying Ping Wang with Chris Lu regional, CO_2 modelling advice. Ian Enting provided guidance on interpreting the $\delta^{13}C$ spatial gradients.

Appendix A

Trace Gas Data processing: The analyses for both dC/dt and ΔC are based on monthly average mixing ratios (or $\delta^{13}C$ isotopic ratios) obtained from a smooth curve through individual flask data (typically 4 month^{-1}) with combined harmonic (seasonal) and 80-day smoothing spline (Thoning et al., 1989). At Cape Grim, selected data represent strong near-surface winds (>5ms^{-1}, 164 m above sea level) with trajectories (typically >10 days) over the Southern Ocean; at Mauna Loa samples are collected in moderate down-slope winds; South Pole samples are selected to avoid local (station) contamination. Conventional smoothing splines through de-seasonalised baseline-selected concentration data, with 50% attenuation at 22-months, are differentiated to provide dC/dt since 1992; Francey et al. (2016) discuss dC/dt uncertainties. Annually averaged ~80-day smoothed monthly baseline concentration data are used to provide ΔC with near-annual time resolution, i.e. potential ambiguity between seasonality and inter-annual variation is addressed differently by dC/dt and ΔC. CSIRO and NOAA data are processed identically. Scripps data used here are monthly data that are seasonally adjusted and filled (http://scrippsco2.ucsd.edu/data/).

(Note: Using the spatial differences from individual laboratories effectively removes most calibration issues that can complicate high precision comparisons of data between laboratories).

Appendix B

Laboratory Differences in $\delta^{13}C$ data:

The $\delta^{13}C$ in CO_2 are a 'reduced ratio' of $^{13}C/^{12}C$, for sample s and reference r:

$$\delta^{13}C_s = \left({}^{13}C_s / {}^{12}C_s - {}^{13}C_r / {}^{12}C_r\right) / \left({}^{13}C_r / {}^{12}C_r\right)$$

Mass conservation in ^{13}C is approximated using the product of C and $\delta^{13}C$ (e.g. Tans et al., 1993).

The assumption of independence between C and $\delta^{13}C$ measurements is marginally compromised by the use of the N_2O/CO_2 ratio to correct the $\delta^{13}C$ for mass spectrometer split resolution (e.g. Allison and Francey, 2007). The difference in 2009 and 2010 corrections to $\Delta\delta^{13}C$ is <0.0007 ‰ compared with the magnitude of ~0.029 ‰ for the 2009–2010 step (Colin Allison personal communication).

Flask CO_2 differences between NOAA and CSIRO same-air comparisons at cgo since 1992 are 0.11±0.13 ppm (Masarie et al., 2001; Francey et al., 2015). It is assumed that the mean offset cancels in mlo-cgo differences. This implies that the maximum $\delta^{13}C$ measurement error due to flask air contamination should be less than 0.005 ‰.

Exact reasons for the varying quality of $\delta^{13}C$ programs in Fig. 6 are not known. However, reduced scatter in CSIRO program is possibly related to feedback from regular quality assessment provided by unique method redundancy (Allison and Francey, 2007). The data in this report involve small subsamples of chemically dried whole flask air, from which CO_2 is extracted and analysed using a fully automated Finnigan-Matt 602 D Mass Spectrometer (MS) with MT Box-C extraction accessory, and bracketed by extractions and analysis of cgo long-lived baseline air standards in high-pressure cylinders. Over most of the two decades a parallel cgo program involved unique large-sample *in situ* extraction of CO_2, which is returned and analysed on the same MS, but relative to independently propagated pure CO_2 standards.

Despite inadequate support to maintain future quality control in the CSIRO isotope program, a 2013 thorough quality audit occurred in the context of comparing recent and 1990s $\delta^{13}C$ measurements of ice core air (Rubino et al. 2013).

Appendix C

Atmospheric Transport: In contrast to the situation in Figure 4c, the average 300hPa zonal wind for July 2008 to June 2009, shown in Fig. 4d, has equatorial westerlies between the date line and 120W. The westerly duct is open and NH extra-tropical Rossby waves, including the Himalayan wave-train, are able to penetrate into the SH. Correlation analysis (Frederiksen and Webster, 1988) indicates increased upper tropospheric transient kinetic energy near the equator with facilitated IH transport of trace gases. Here we have focused on the 300hPa level, but our results apply in broad terms to most of the upper troposphere. In particular, the correlation of the SOI with the zonal wind in the westerly duct region (Fig. 4a) applies between 500hPa and 70hPa with similar strength between 300 and 100hPa and reducing at the upper and lower levels. Again, the structure of the (July 2008 to June 2009) minus (July 2009 to June 2010) zonal wind difference (Fig. 4b) is largely equivalent barotropic with similar strength between 300hPa and 100hPa and reducing at the upper and lower levels. Northern winter (DJF)

differences for 2008/2009 minus 2009/2010 are circa twice as strong in the westerly duct region as those in Fig. 4b.

The Prabir atmospheric transport modelling (Prabir, 2015) relies on measurements of SF_6 to support the transport parameterisation. Our early examination of such synthetic species with respect to the 2009/2010 event was inconclusive. While we can demonstrate a considerable degree of systematic behaviour in the variation in baseline monthly CO_2 IH differences, by comparison the synthetics were found to have much larger scatter, though significant precision improvements have occurred since 2011 (Paul Krummel, personal communication). Furthermore, over the period of most concern, we found little agreement between the NOAA HATS SF_6 data (http://www.esrl.noaa.gov/gmd/hats/combined/SF6.html), and equivalent data from the AGAGE network (https://agage.mit.edu/) in month-to-month, or inter-annual variability about the long term increase in IH difference. The use of past SF_6 to calibrate the inter-hemispheric transport may well be adequate for the long-term model mean transport, but fail to adequately constrain past irregular periods such as 2009/2010, or the similar historic events.

References

Allison, C. E. and Francey, R. J.: Verifying southern hemisphere trends in atmospheric carbon dioxide stable isotopes, J. Geophys. Res., 112(D21304), doi:10.1029/2006JD007345, 2007.

Ashfold, M. J., Pyle, J. A., Robinson, A. D., Meneguz, E., Nadzir, M. S. M., Phang, S. M., Samah, A.A., Ong, S., Ung, H. E., Peng, L. K., Yong, S. E., and Harris, N. R. P.: Rapid transport of East Asian pollution to the deep tropics, Atmos. Chem. Phys., 15, 3565–3573, doi:10.5194/acp-15-3565-2015, 2015.

Boden, T. A., Marland, G. and Andres, R. J.: Global, regional, and national fossil-fuel CO_2 emissions. Carbon Dioxide Information Analysis Center, 2010. http://cdiac.ornl.gov/trends/emis/overview.html

Ciais, Ph., Reichstein, M., Viovy, N., Granier, A., Ogée, J., Allard, V., Aubinet, M., Buchmann, N., Bernhofer, Chr., Carrara, A., Chevallier, F., De Noblet, N., Friend, A. D., Friedlingstein, P., Grùnwald, T., Heinesch, B., Keronen, P., Knohl, A., Krinner, G., Loustau, D., Manca, G., Matteucci, G., Miglietta, F., Ourcival, J. M., Papale, D., Pilegaard, K., Rambal, S., Seufert, G., Soussana, J. F., Sanz, M. J., Schulze, E. D., Vesala, T., and Valentini, R.: Europe-wide reduction in primary productivity caused by the heat and drought in 2003, Nature 437, 529-533, doi: 10.1038/nature03972, 2005.

Denning, A. S., Takahashi, T., and Friedlingstein, P: Can a strong atmospheric CO_2 rectifier effect be reconciled with a ‘‘reasonable’’ carbon budget? Tellus, 51B, 249–253, 1999.

Dlugokencky, E. J., Lang, P.M., Masarie, K.A., Crotwell, A.M., and Crotwell, M.J.: Atmospheric Carbon Dioxide Dry Air Mole Fractions from the NOAA ESRL Carbon Cycle Cooperative Global Air Sampling Network, 1968-2013, Version: 2014-06-27, 2014. Path: ftp://aftp.cmdl.noaa.gov/data/trace_gases/co2/flask/surface/

Enting, I. G., Trudinger, C. M., Francey, R. J., and Granek, H.: Synthesis inversion of atmospheric CO_2 using the GISS tracer transport model. CSIRO Division of Atmospheric Research Technical Paper No. 29, 551.51120287, CSIRO Australia, 1993

Enting, I. G.: Inverse Problems in Atmospheric Constituent Transport, Cambridge Univesity Press, 0521812100, 2006.

Francey, R. J., Trudinger, C. M., van der Schoot, M., Law, R. M., Krummel, P. B., Langenfelds, R. L., Steele, L. P., Allison, C. E., Stavert, A. R., Andres, R. J. and Rödenbeck ,

C.: Atmospheric verification of anthropogenic CO_2 emission trends, Nat. Clim. Ch. 3, 520-524, doi:10/1038/nclimate1817, 2013.

Francey, R. J., R. L. Langenfelds, L. P. Steele, P. B. Krummel and M. van der Schoot, Bias in the biggest terms in the global carbon budget?: In: Krummel P. B. and Derek, N., editors. Baseline Atmospheric Program Australia 2011-2013. [Melbourne]: Australian Bureau of Meteorology in cooperation with CSIRO Division of Atmospheric Research, 2016 (in press).

Frederiksen, J.S. and Webster, P.J.: Alternative theories of atmospheric teleconnections and low-frequency fluctuations, Rev. Geophys., 26, 459-494, 1988.

Giglio, L., Randerson, J. T., and van derWerf, G. R.: Analysis of daily, monthly, and annual burned area using the fourth-generation global fire emissions database (GFED4), J. Geophys. Res. Biogeosci., 118, 317–328, doi:10.1002/jgrg.20042, 2013. http://www.falw.vu~gwerf/GFED/GFED4/tables/GFED4_BETA_CO2.txt

Keeling, R. F., Piper, S. C., Bollenbacher, A. F., and Walker, J. S.: Atmospheric CO_2 records from sites in the SIO air sampling network. In Trends: A Compendium of Data on Global Change. Carbon Dioxide Information Analysis Center, Oak Ridge National Laboratory, U.S. Department of Energy, Oak Ridge, Tenn., U.S.A., doi: 10.3334/CDIAC/atg.035, 2009.

Law, R. M. Kowalczyk and Wang Y-P, Using atmospheric CO_2 data to assess a simplified carbon-climate simulation for the 20th century, Tellus, 58B, 427–437, 2006.

Law, R.M., 2014. http://www.climatescience.org.au/sites/default/files/LAW_COECSS_Sep2012.pdf

Lloyd, J., and Farquhar, G. D.: ^{13}C discrimination during CO_2 assimilation by the terrestrial biosphere, Oecologia, 99, 201–215, 1994.

Locatelli, R., Bousquet, P., Chevallier, F., Fortems-Cheney, A., Szopa, S., Saunois, M., Agusti-Panareda, A., Bergmann, D., Bian, H., Cameron-Smith, P., Chipperfield, M. P., Gloor, E., Houweling, S., Kawa, S. R., Krol, M., Patra, P. K., Prinn, R. G., Rigby, M., Saito, R., and Wilson, C.: Impact of transport model errors on the global and regional methane emissions estimated by inverse modelling, Atmos. Chem. Phys., 13, 9917-9937, doi:10.5194/acp-13-9917-2013, 2013.

Masarie, K. A., Langenfelds, R. L., Allison, C. E., Conway, T. J., Dlugokencky, E. J., Francey, R. J., Novelli, P. C., Steele L. P., Tans P. P., Vaughn B., and White, J. W. C.:

NOAA/CSIRO Flask Air Intercomparison Experiment: A strategy for directly assessing consistency among atmospheric measurements made by independent laboratories. J. Geophys. Res., 106 (D17): 20445-20464, 2001.

Matsueda, H., Machida, T., Sawa, Y., and Niwa, Y.: Long-term change of CO_2 latitudinal distribution in the upper troposphere, Geophys. Res. Lett., 42, 2508-2514, doi:10.1002/s014GL062768, 2015.

McGregor, J. L., and Dix, M. R. An updated description of the conformal-cubic atmospheric model. High Resolution Simulation of the Atmosphere and Ocean, Hamilton, K. and Ohfuchi, W., Eds., Springer, 51-76, 2008.

Miyazaki, K., Patra, P. K., Takigawa, M., Iwasaki, T., and Nakazawa, T.: Global-scale transport of carbon dioxide in the troposphere, J. Geophys. Res., 113, D15, doi:10.1029/2007JD009557, 2008.

Page, S. E., Hoscilo, A., Langner, A., Tansey, K. J., Siegert, F., Limin, S. H., and Rieley, J. O.: Tropical peatland fires in Southeast Asia. In: M. A. Cochrane (Eds). Tropical Fire Ecology: Climate Change, Land Use and Ecosystem Dynamics. Springer-Praxis, Heidelberg, Germany, 263-287, 2009.

Patra P.: Biogeosciences Discuss., 12, C6469–C6469, 2015.

Peters, G. P., Marland, G., Le Quéré, C., Boden, T., Canadell, J. G., and Raupach, M. R., Rapid growth in CO_2 emissions after the 2008–2009 global financial crisis, Nat. Clim. Ch. 2, 1-4, doi:10.1038/nclimate1332, 2012.

Peylin, P., R. M. Law, K. R.Gurney, F. Jacobson, A. R. Maki, Y. Niwa, P. K. Patra, W. Peters, P. J. Rayner, C. Rödenbeck, I. T.van der Laan-Luijkx, and X. Zhang, Global atmospheric carbon budget: results from an ensemble of atmospheric CO_2 inversions, *Biogeosciences* 10, 6699-6720, doi:10.5194/bg-10-6699-2013, 2013.

Poulter, B., Frank, D., Ciais, P., Myneni, R. B., Andela, N., Bi, J., Broquet, G., Canadell, J. G., Chevallier, F., Liu, Yi Y., Running, S. W., Sitch, S. and van der Werf, G. R.: Contribution of semi arid ecosystems to inter-annual variability of the global carbon cycle, Nature, 509, 600–603, doi:10.1038/nature13376, 2014.

Poulter, B. Biogeosciences Discuss., 12, C7009–C7011, 2015.

Rayner, P. J., Law, R. M., Allison, C. E., Francey, R. J., Trudinger, C. M., and Pickett-Heaps, C.: Interannual variability of the global carbon cycle (1992–2005) inferred by inversion of

atmospheric CO_2 and $\delta^{13}CO_2$ measurements, Global Biogeochem. Cy., 22, GB3008, doi:10.1029/2007GB003068, 2008.

Randerson, J. T., Collatz, G. J., Fessenden, J. E., Munoz, A. D., Still, C. J., Berry, J. A., Fung, I. Y., Suits, N., and Denning, A. S.: A possible global covariance between terrestrial gross primary production and ^{13}C discrimination: Consequences for the atmospheric ^{13}C budget and its response to ENSO, Global Biogeochem. Cycles, 16, 1136-1152, doi:10.1029/2001GB001845, 2002.

Stephens, B. B., Gurney, K. R., Tans, P. P., Sweeney, C. Peters, W. et al., The vertical distribution of atmospheric CO_2 defines the latitudinal partitioning of global carbon fluxes, Science, 316, 1732-1735, 2007.

Stephens, B. B., Brailsford, G. W., Gomez, A. J., Riedel1, K., Mikaloff Fletcher, S. E., Nichol1, S., and Manning, M., Analysis of a 39-year continuous atmospheric CO2 record from Baring Head, New Zealand, Biogeosciences, 10, 2683–2697, doi:10.5194/bg-10-2683-2013, 2013.

Tans, P. P., Berry, J. A., and Keeling, R. F.: Oceanic ^{13}C data: A new window on CO_2 uptake by the oceans, Global Biogeochem. Cy., 7, 353– 368, 1993.

Thoning, K. W., Tans, P. P., and Komhyr, W. D.: Atmospheric carbon dioxide at Mauna Loa observatory, 2, Analysis of the NOAA/GMCC data, 1974-1985, J. Geophys. Res., 94, 8549-8565, 1989.

Webster, P. J., and Holton, J. R.: Cross-equatorial response to mid-latitude forcing in a zonally varying basic state, J. Atmos. Sci., 39, 722-733, 1982.

Webster, P. J., and Chang, H.-R.: Equatorial energy accumulation and emanation regions: Impacts of a zonally varying basic state, J. Atmos. Sci., 45, 803-829, 1988.

Figure 1. North-South differences and growth rates in CO_2 since 1990:

(a) On the left axis, annual average (Jan-Dec) ΔC (ppm) from three programs, CSIRO, NOAA (mlo-cgo) and SIO (mlo-spo), plotted mid-year. On the right axis are reported anthropogenic emissions (dashed line), with the Francey et al. (2013) suggested correction (shaded), scaled so that the overall slope is similar to that from the long term mlo-spo SIO record. (b) CSIRO (mlo, cgo, spo) and NOAA (mlo) growth rates, dC/dt, plotted mid- month. See Methods for detail.

Figure 2. North-South CO_2 differences using other NH sites from the NOAA network:

(NH site minus cgo) using annual average baseline data (calendar year, plotted mid-year). Latitude and Longitude of sites are provided in the legend.

Figure 3. Monthly mlo-cgo CO_2 differences:

CSIRO Data of Fig. 1a are plotted monthly to better examine the onset of the 2009–2010 step (see text).

Figure 4: The equatorial upper troposphere duct:

(a) Correlation over the annual cycle of 1949-2011 upper tropospheric winds (300 hPa) with the Southern Oscillation Index (SOI), with strongest correlation in the equatorial Pacific duct.

(b) The difference between open and closed equatorial duct patterns of Figs. 4d and 4c, showing similarity to the long-term correlation pattern in Fig. 4a.

(c) July 2009 to June 2010 ‘closed-duct’ pattern with 300 hPa easterly zonal wind in the equatorial duct.

(d) July 2008 to June 2009 ‘open-duct’ pattern with 300 hPa westerly zonal winds in the equatorial duct.

Figure 5. Monthly inter-hemispheric exchange for CSIRO trace gas species:

The top panel shows monthly u_{duct} (300hPa, 5N to 5S, 140W to 170W) with red and blue bands indicating El Nino and La Nina periods respectively. The relative strength and duration of NH winter (Oct to Apr) IH mixing is estimated by Σu_{duct}, plotted in January.

The following panels show the relative interhemispheric exchange fluxes ($\Delta C.u_{duct}$), due to Pacific upper level equatorial turbulence, for different CSIRO flask species (CO_2, CH_4, CO and H_2). Black circles indicate 4 months of missing CSIRO flask data from mlo; for CO_2, data from these months are obtained from NOAA records.

Figure 6. Isotopic evidence that inter-hemispheric CO_2 variations are systematic:

The interhemispheric differences $\Delta^{13}CO_2$, represented by $\Delta(C.\delta^{13}C)$ plotted against $\Delta^{12}CO_2$ for a) CSIRO (mlo-cgo), b) NOAA (mlo-cgo) and c) SIO (mlo-spo) flask samples since 1992. (One 2003 NOAA outlier (>5σ), is removed from these plots and regressions.) The linear regression coefficients and correlation coefficients (r^2) are provided for each data set.

Figure 7. Inter-hemispheric mlo-spo differences from the historic Keeling CO_2 record and u_{duct}:

The top panel shows monthly u_{duct} (300hPa, 5N to 5S, 140W to 170W) with red and blue bands indicating El Nino and La Nina periods respectively (left axis). The relative strength and duration of NH winter (Oct to Apr) IH mixing is estimated by Σu_{duct}, plotted in January (right axis).

In the bottom panel annual average mlo-spo ΔC are shown. Red circles indicate occasions when integrated duct transport is <5 ms^{-1}, dashed for >5 ms-1, and smaller circles (in the top panel) when brief closures are not followed by La Niña and there is no detectable ΔC influence.

07.01.2016

fig01

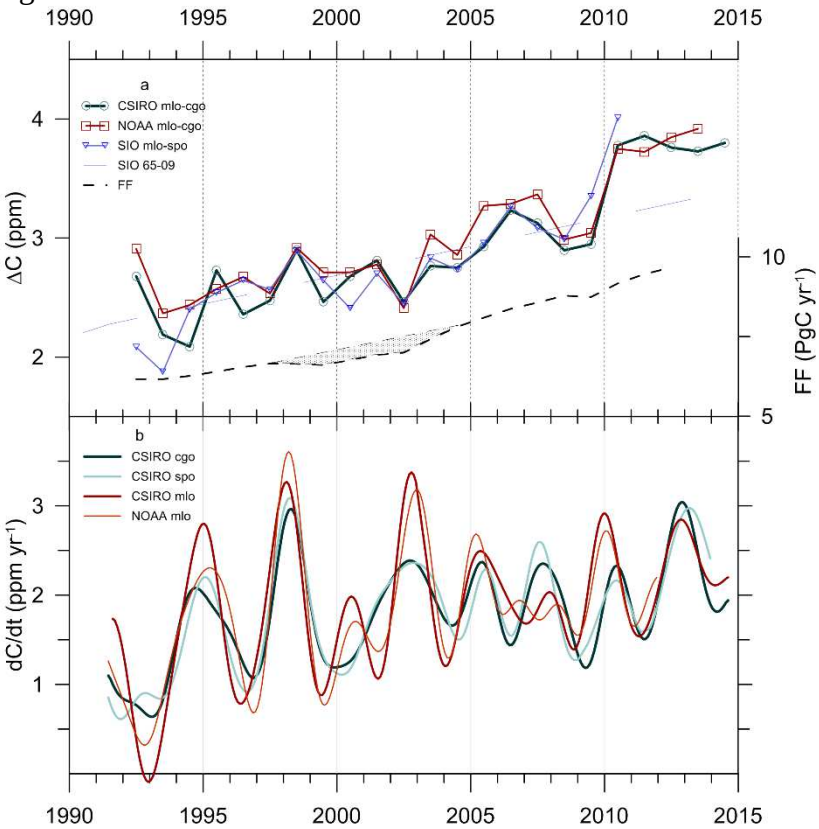

610

07.01.2016

fig02

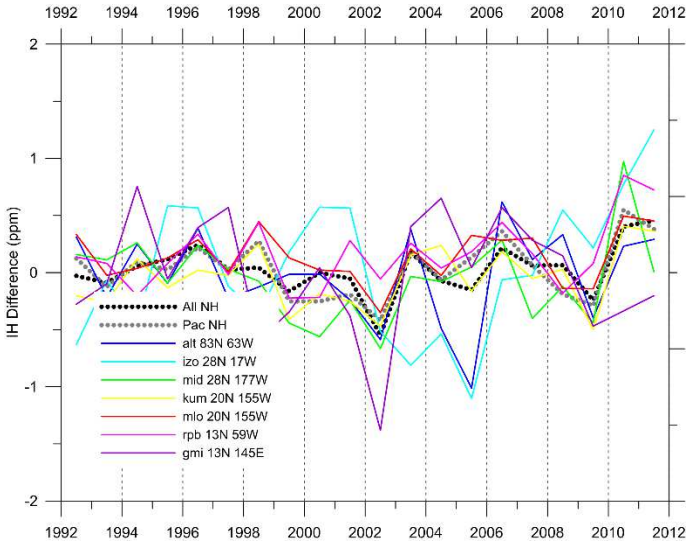

07.01.2016

fig03

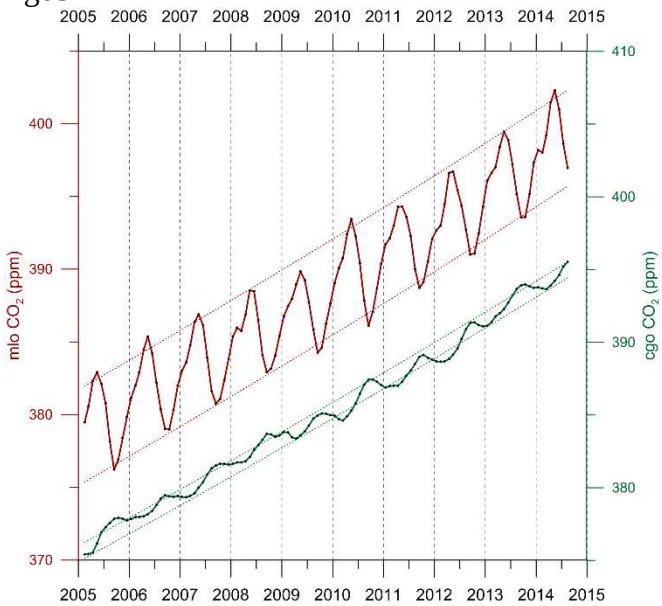

07.01.2016

fig04

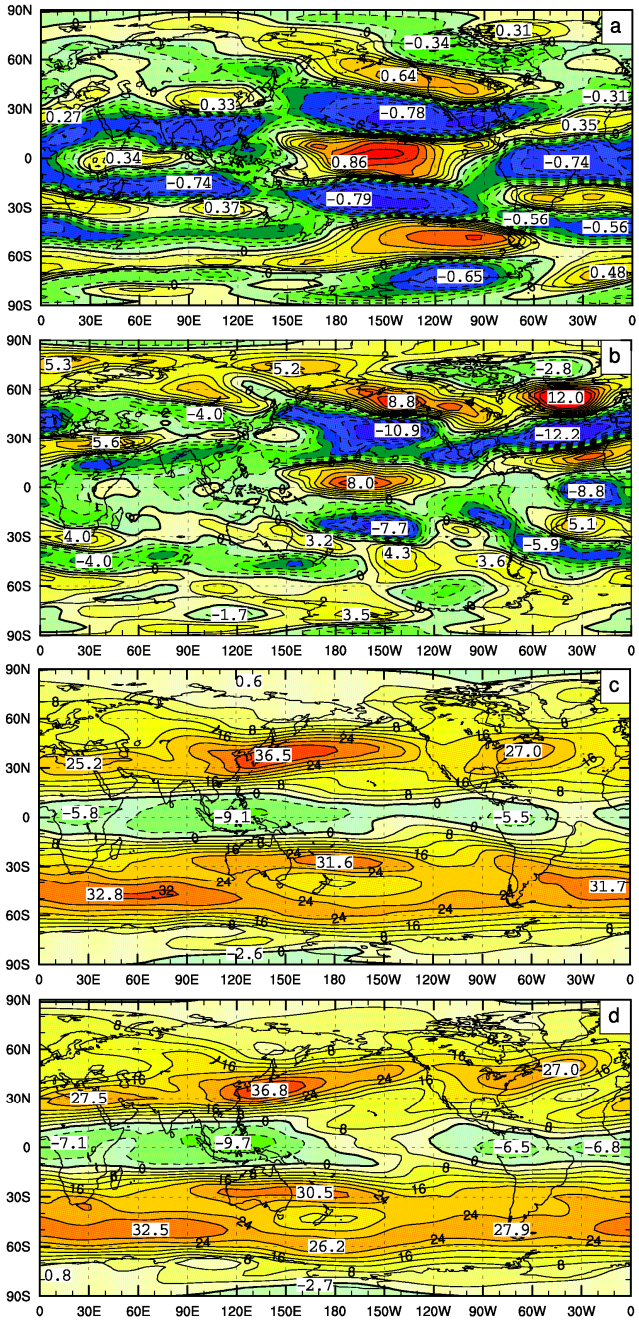

620

07.01.2016

fig05

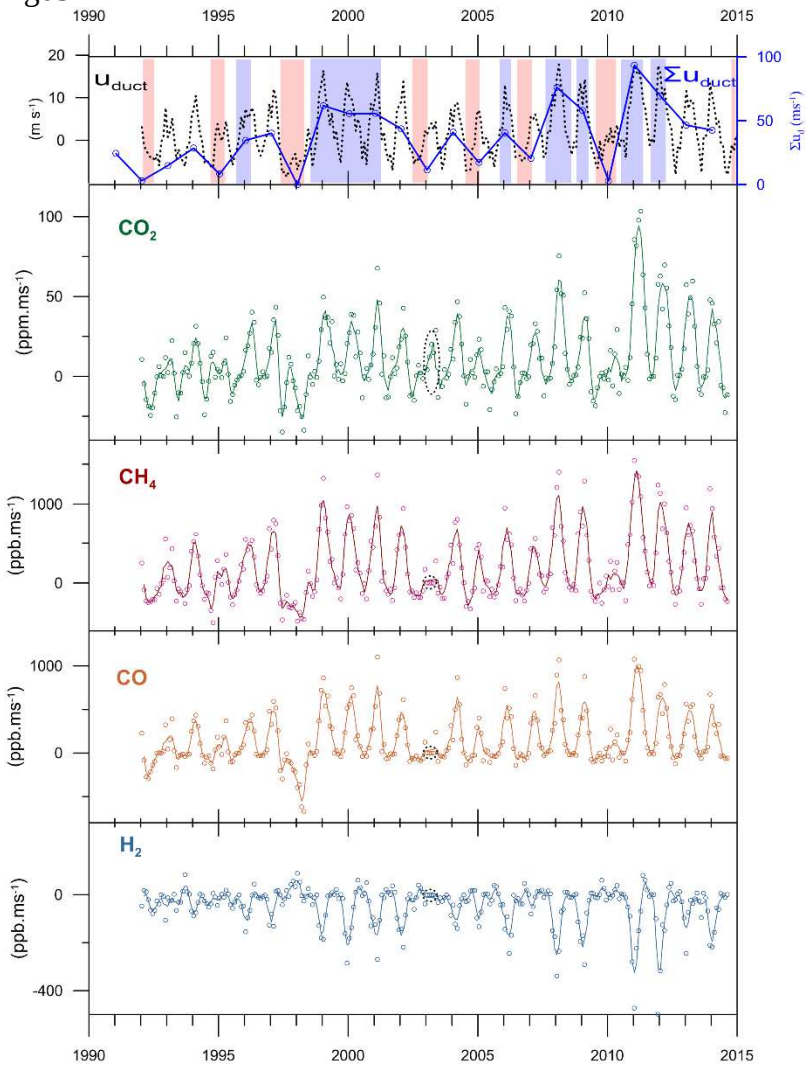

07.01.2016

fig06

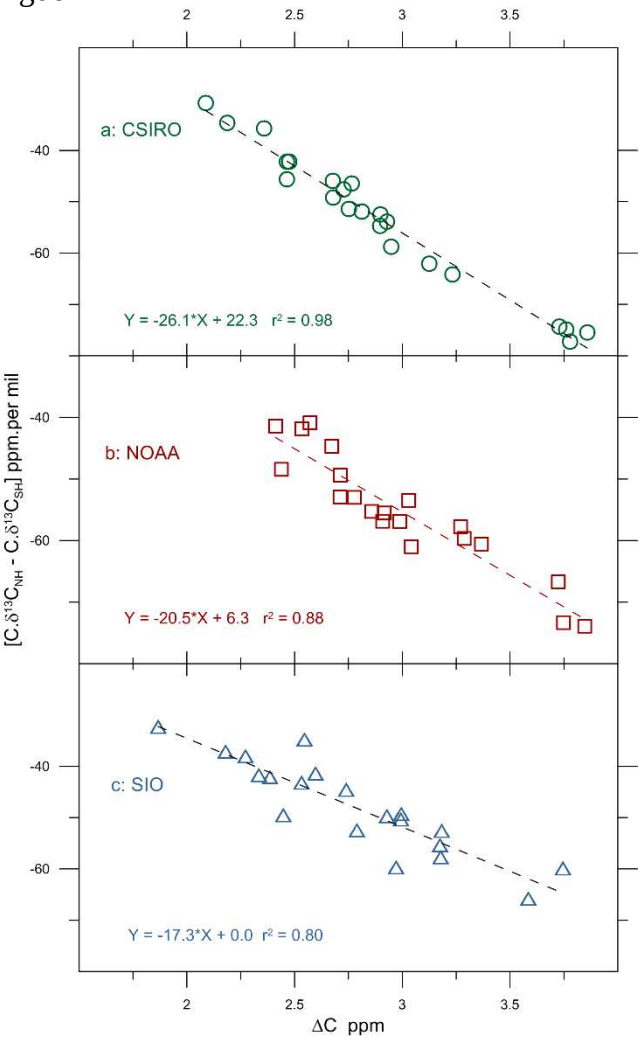

625

07.01.2016

fig07

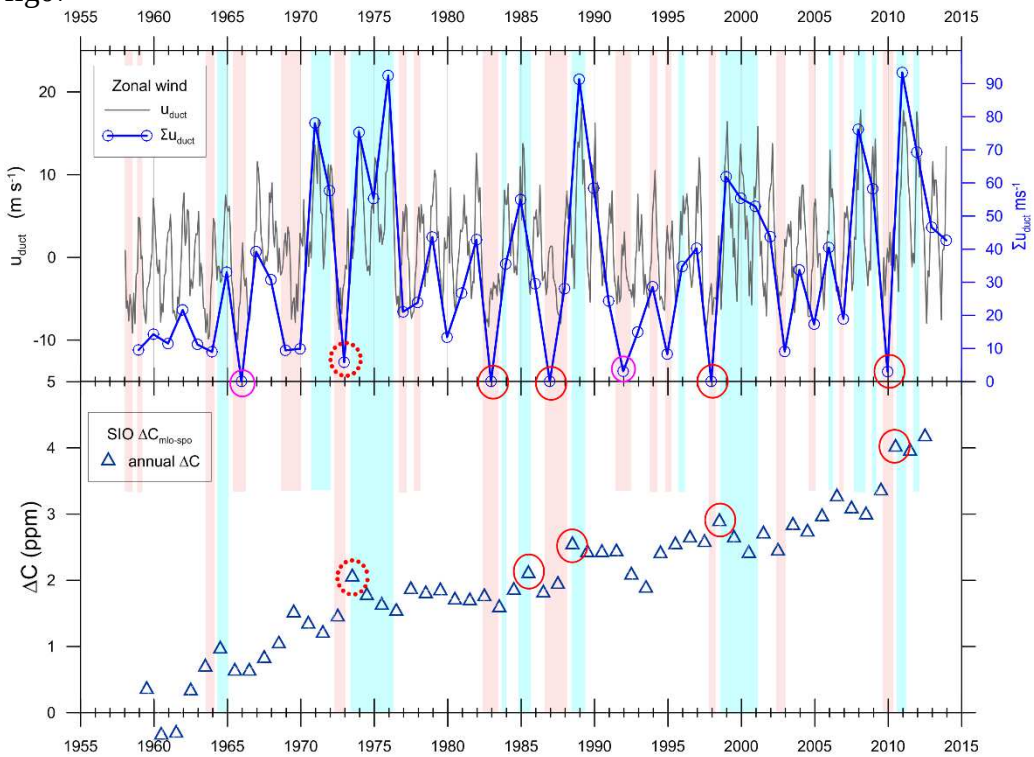

630